Heat Transfer to Solid-Vapor Mixtures of Cryogens below their Triple Points Flowing through Heated Tubes

M. C. JONES, PATRICIA J. GIARRATANO

National Bureau of Standards, Boulder, Colorado

and A. U. SIMPSON

AiResearch Manufacturing Company, Los Angeles, California

Data are presented for wall temperatures and heat transfer coefficients for solid-vapor mixtures of parahydrogen and nitrogen flowing in an electrically heated straight tube of length 40 times its diameter. These are interpreted by the application of flat plate, constant property boundary-layer theory to models in which the solid particle geometrical distribution takes on simple limiting forms. The observed enhancement of the heat transfer coefficient over that for gas alone traveling at the same velocity is qualitatively predicted as a function of a dimensionless heat flux, the Sterman parameter $q_w/\rho_v U\lambda$.

The study described below was conducted in order to obtain information on the flow and heat transfer characteristics of single component, solid-vapor mixtures flowing through rocket engine propellant supply lines and propellant tank vent lines. The mixtures are formed when cryogenic liquid fuels are introduced into lines open to space atmospheres and thus at pressures below 10^{-6} torr. This is well below the triple point pressures of most liquid fuels. Triple point pressures of some common liquids are listed in Table 1. Such circumstances are most commonly encountered during the idle period or restart of an engine and during the accidental venting of liquid from a supply tank and can lead to lines plugged with solid.

In order to obtain basic information on this phenomenon, liquids were expanded through orifices at the entrance of a simple straight tube and then discharged into a chamber under vacuum. Fine suspensions of solids in their own vapor were formed and, under certain heating conditions of the tube, were seen through windows in the vacuum chamber to discharge freely from the tube in a fairly homogeneous column. Under conditions of insufficient heat input, discharge became unsteady and even ceased with the tube temporarily blocked with solid.

TABLE 1. SUMMARY OF TRIPLE POINT TEMPERATURES AND PRESSURES

	Triple Point Temperatures (°K.)	Triple Point Pressure (torr)
parahydrogen	13.8	52.8
nitrogen	63.2	94.1
fluorine	53.5	1.92
oxygen	54.4	1.14
water	273.16	4.58
carbon dioxide	216.6	3885.2

The goals of this study were to establish heating conditions which would permit free discharge of the solid-vapor mixtures and to measure heat transfer coefficients for heat input through the tube wall. The latter are, in fact, unique two-phase, forced convection heat transfer results, but are quite related to more familiar studies of inert solid-in-gas suspensions (*1* to *5*).

Previous studies of flow and heat transfer to gas-inert solids mixtures were motivated by the desire to improve the heat transfer coefficient of a gas stream. Experimental data of various workers including the authors themselves were compared by Farbar and Depew (*1*) for various solids (glass spheres, catalysts, etc.) suspended in air streams. In summary, their work showed that the pure gas heat transfer coefficient could be enhanced, enhancement increasing with the proportion of solids present and decreasing with increase of particle size. Particles greater than 200μ did not appear to affect the heat transfer while 30μ particles gave up to a fourfold enhancement for solids to gas mass flow ratios up to 10. For the smaller particles, however, at mass flow ratios less than 4 a decrease in heat transfer coefficient below the pure gas value was noted. Similar observations were reported by Tien and Quan (*2*). They worked at mass flow ratios less than 3.5 with 30 and 200μ particles in both glass and lead. Only for the 30μ glass particles was significant enhancement noted; significantly, glass has a volumetric heat capacity about 30% higher than that of lead.

Abel, et al. (*3*) conducted experiments with micronized graphite (particles in the size range $1 < D_p < 10\mu$) suspended in helium and nitrogen gas at mass flow ratios up to about 3. Only marginal enhancement of heat transfer was obtained, but the meaning of the results is obscured by the occurrence of deposition of graphite on walls of the test section.

Theoretical expressions for heat transfer coefficients for gas-inert solid flow have been derived. In a simplified treatment of heat transfer in fully developed turbulent flow,

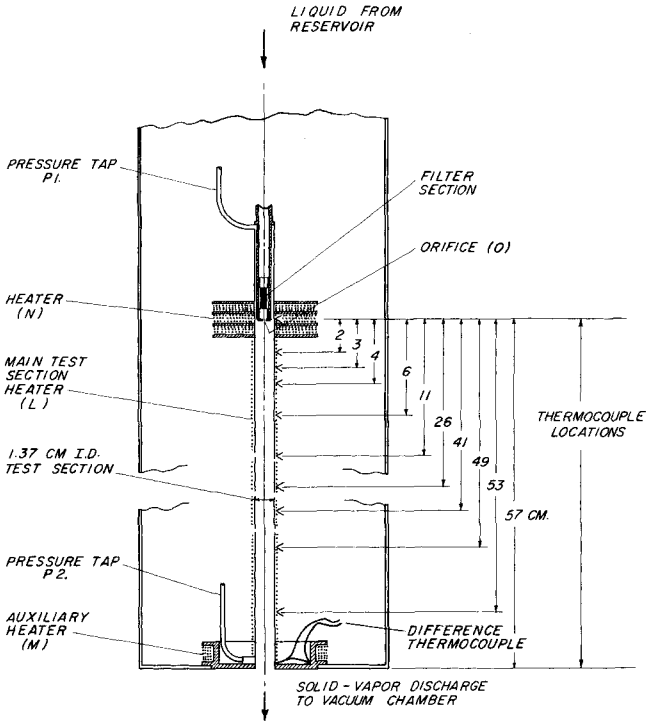

Fig. 1. Test section, showing heaters and locations of thermocouples.

with uniform distribution of very small particles and an unperturbed velocity profile, Tien (*4*) showed that the enhancement was proportional to the factor

$$\left(1+\frac{\rho_p C_{p,p}}{\rho_v C_{p,v}}\right)$$

In a laminar boundary-layer analysis Edelman (*5*) derived the enhancement factor

$$\left(1+\frac{\rho_p C_{p,p}}{\rho_v C_{p,v}}\right)^{1/3}\left(1+\frac{\rho_p}{\rho_v}\right)^{1/6}$$

Again, uniform particle distribution was assumed.

From this work the prognosticated major effect of the presence of inert particles is that they act as heat sinks for the vapor and, insofar as they do not constitute a hydrodynamic disturbance, they prolong the entrance region and consequently enhance heat transfer.

For subliming solid-vapor mixtures, only the previous work of Jones, et al. (*6*) is available. Preliminary studies were made of heat transfer to solid-vapor mixtures of parahydrogen below its triple point pressure flowing through a short (length = 13 diam.) uniformly heated tube. Enhancement was again observed and a dependence upon heat flux noted. A correlation was suggested in which a dimensionless heat flux, the Sterman parameter, was used. This will be discussed more fully. In that work only hydrogen data were reported since it was found impossible to obtain free flow of solid-vapor mixtures of nitrogen in the same apparatus.

In the present study a tube of 40 diam. length was used and was investigated for both parahydrogen and nitrogen. Free flow was achieved by concentrating heat in the vicinity of the entrance orifice. The mixtures studied are characterized by a particle size range between 10 and 500μ with an estimated most probable size of about 30μ. The quality of the mixtures at the tube inlet was calculated to lie between 25 and 30% mass of vapor for assumed isenthalpic expansion through the orifice.

EXPERIMENTAL APPARATUS AND PROCEDURE

The solid-vapor mixtures were investigated in a modification of an apparatus previously described by Jones, et al. (*6*). Briefly, the mixtures were formed by forcing subcooled liquids downwards through an orifice at the inlet end of a straight, vertical, heated tube situated in a large vacuum chamber, which was held at pressures below the triple point of the liquid. The major modifications were:

1. The use of a continuous flow rather than batch operation.
2. Automatic control of the vacuum chamber pressure.
3. The use of a vacuum jacket to insulate the test section.
4. Redesign of the now larger test section with more complete instrumentation.

Details of the test section, instrumentation and procedure follow.

Test Section

The details of the test section are shown in Figure 1. It was a vacuum insulated Inconel tube of 1.37 cm. internal diameter (9/16 in. O.D., 0.012 in. wall) having a length to diameter ratio of approximately 40 between the inlet orifice and the end of the tube.

Ten calibrated chromel-constantan thermocouples, located as indicated in Figure 1 were used to measure wall temperatures; three heaters on the test section were used as follows:

1. Main test-section heater (wound uniformly and noninductively) along the length of the tube to supply heat to the solid-vapor mixture flowing in the test section.
2. Auxiliary heater at the lower end of the test section to prevent heat loss from the bottom of the warm tube wall to the cold vacuum insulating jacket. An eleventh difference thermocouple located between the tube wall and the insulating jacket flange provided an error signal for a temperature controller which supplied power to this heater and continuously compensated for the heat loss.
3. Heater adjacent to discharge orifice to prevent caking of solid on the tube wall adjacent to the orifice.

Pressure taps P1 and P2 located at the top and bottom of the test section were used for measuring static pressure drop along the tube during free flow of the solid-vapor mixture.

Instrumentation

A data acquisition system consisting of a digital voltmeter, amplifier, scanner, and printer was used for measuring and

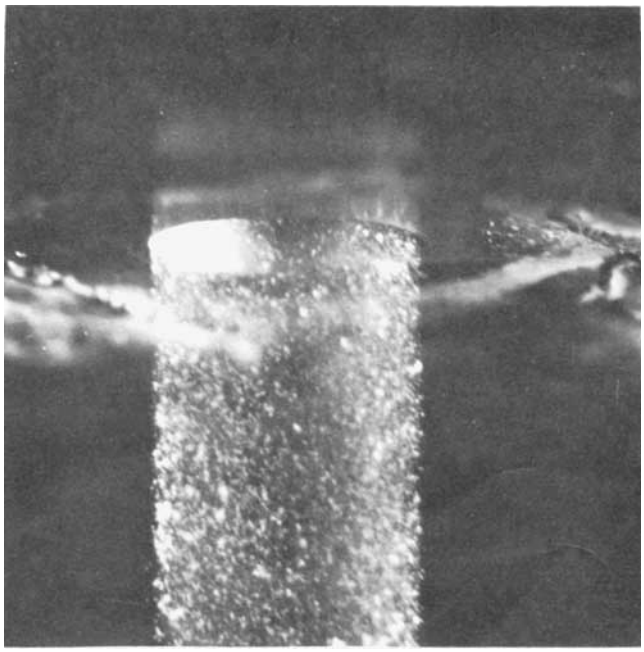

Fig. 2. Discharge of solid-vapor mixture of hydrogen, (q_w = 0.29 W/sq. cm., N_{Sr} = 0.0015).

recording all voltages and currents. These included heater voltages and currents, thermocouple electromotive forces and the voltage drop and current through a germanium resistance thermometer located inside a small liquid reservoir above the orifice. This reservoir also contained ahe thermocouple reference junctions.

Flow rates were measured by means of a calibrated flow orifice, the pressure drop being read on a water manometer. The flow orifice was submerged in a precooler to assure single-phase liquid flow.

Vacuum chamber pressure was measured by an absolute pressure mercury manometer, and a specially designed mercury U-tube manometer capable of indicating small pressure drops was used to measure the pressure drop along the test section.

Photographs of the emerging solid-vapor stream were taken using a commercial microflash unit, which had a flash duration of 0.3×10^{-6} sec. and a specially constructed camera consisting of a lens, a 1 m. expansion bellows and film holder. Because it was impractical to locate the camera close to the discharging stream inside the vacuum chamber, the special camera arrangement was necessary to obtain sufficient resolution of the solid particles.

Procedure

In order to carry out heat transfer measurements the vacuum chamber was first evacuated to below the triple point pressure of the test fluid and set on automatic control. Liquid was then admitted to the flow system achieving cooldown in about 15 min. At the first sight of solid emerging from the end of the test section power was applied to heaters L and N. Finally, when steady conditions were achieved power was applied to heater M, which was placed under automatic control when zero temperature difference was indicated between the end of the test section and the vacuum jacket flange.

For all runs with a single fluid the power input to heater N was held constant at a level at which caking of solid did not occur and a steady, continuous, homogeneous, solid-vapor mixture emerged from the end of the tube. Power to heater L was varied at will to obtain the variation of wall temperatures with heat flux. After a power adjustment on L usually five or ten minutes were required in order to obtain steady wall temperatures. At this time the data recording system was set in operation and all voltages recorded in sequence for five cycles of the scanner at a rate of about one reading per second. Computations were based on the average of the five sets of readings.

Flow rates were adjusted by either varying the supply dewar driving pressure or by changing the orifice size.

RESULTS

Typical photographs of the solid-vapor mixture discharging from the end of the test section are shown in Figures 2 and 3 for hydrogen. The absence of visible solid particles in the vicinity of the wall is clearly evident in Figure 3 where the heat flux was three times that for Figure 2. Photographs also indicated that a wide distribution of particle sizes existed in the solid-vapor stream ranging from 10 to approximately 500μ. The limits on particle size are wide since it was not possible in all cases to determine whether some of the particles being measured were individual or optically superimposed particles. Particles less than 10μ could not be seen clearly with the photographic resolution available.

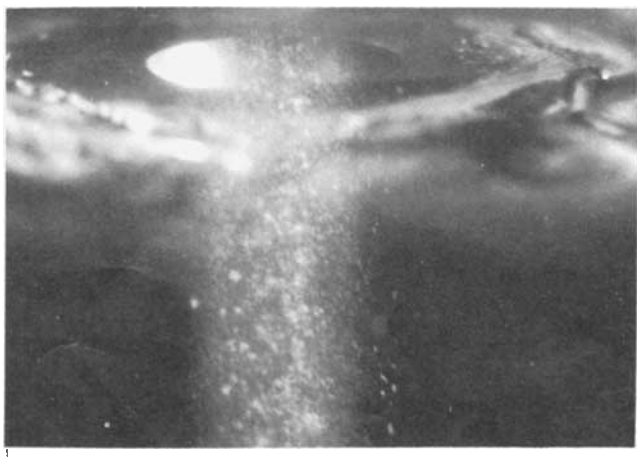

Fig. 3. Discharge of solid-vapor mixture of hydrogen, (q_w = 0.93 W/sq. cm., N_{Sr} = 0.0035).

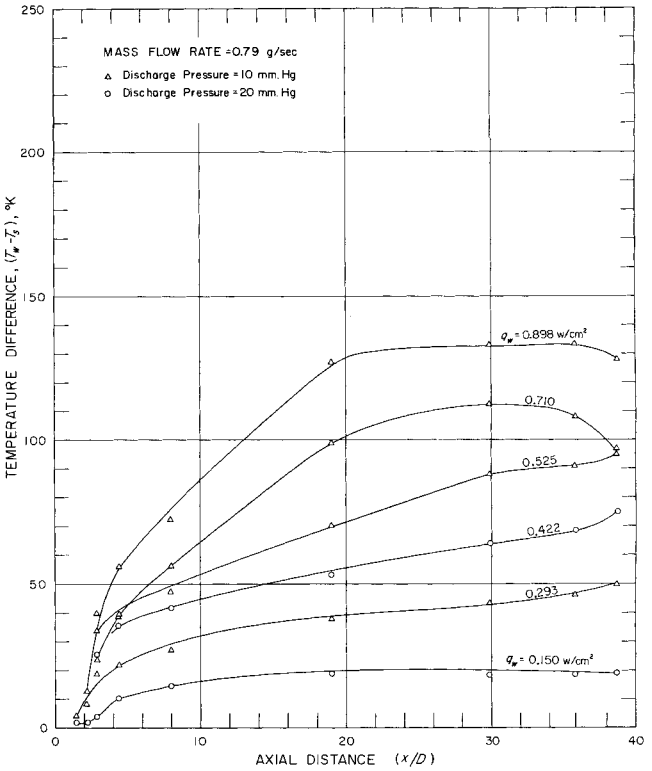

Fig. 4. Experimental temperature difference profiles for hydrogen with q_w as parameter—low flow rate.

Selected temperature difference ($T_w - T_s$) profiles are given in Figures 4 and 5 for hydrogen and Figures 6 and 7 for nitrogen. The inside wall temperature, T_w, was calculated by correcting measured outside wall temperatures for temperature drop through the tube wall. The bulk fluid temperature at a given station was taken as the saturation temperature, T_s, corresponding to the pressure in the tube at that point, there being no means to actually measure it. Pressures at points between P_1 and P_2 were interpolated using compressible flow equations.

The heat flux to the fluid was calculated from the measured electrical power input, taking into account axial conduction along the tube (based on measured wall temperatures) and radiation losses.

The heat flux uncertainties were ± ½%; the uncertainties in the temperature difference were less than ± 5% for approximately 90% of the runs, the worst uncertainties being ± 25 to ± 150% at low heat fluxes (< 0.02 W/sq.cm.) for hydrogen data points. The uncertainties in temperature difference were almost entirely due to a tendency of the wall temperatures to drift randomly during a run. The arithmetic average of all the measured values (5 readings per datum point taken over a 2½ min. interval) were used in the reported results.

In the discussion below it has been convenient to illustrate the results by a plot of the enhancement factor, f, vs. Sterman parameter, N_{Sr}. The estimated uncertainties in these quantities are ± 10% and ± 1% respectively for

most of the runs, the worst values for f being $\pm$ 30 to $\pm$ 155% at $N_{Sr} < 0.0003$ due to large uncertainties in $(T_w - T_s)$ at low heat fluxes.

HEAT TRANSFER THEORY

A complete theoretical description of heat transfer coefficient for the subliming, solid-vapor mixtures investigated in this work would treat momentum and energy transport for the two phases, particle and vapor, in the presence of free stream turbulence, particle transport, vaporization, compressibility effects, and temperature dependent transport properties. Such a general treatment is not yet available and the interpretation of the experimental results must proceed from simplified analyses. Such analyses at this stage of knowledge have the advantage of separating out dominant effects and permitting some insight into the total process.

For the present treatment it was decided to use a boundary-layer technique for laminar, incompressible, constant property flow over a flat plate with constant heat flux and investigate perturbations of the well known single phase results by the presence of vaporizing solid particles. It was considered that, being an entrance region with free stream turbulence enhanced by that from the orifice, the flat plate laminar boundary-layer assumptions would be particularly appropriate up to the point of boundary-layer transition.

A single size particle was chosen representing an average particle. For the geometrical distribution of particles two extreme cases were considered. In the first, a uniform density of particles was assumed throughout. In the second, it was assumed that particles exist only outside the thermal boundary layer. For the velocity distribution of the particles it was decided to treat only the case where no relative velocity exists between the phases, as would be the case of sufficiently small particles.

The von Kármán approximate integral method (7) was used to derive approximate expressions for the heat transfer coefficient. Treating the particle phase as a continuum, Simpson (8) derived the basic continuity, momentum, and energy equations for the two phases separately and the mixture. In these equations the average solid phase density is described by a function ρ_p while the specific density of the solid is a constant, $\tilde{\rho}_p$. The major difference between the conservation equations for a vapor in the presence of the particle phase and a pure vapor or gas is that the former contains an energy sink and a mass source. The mass source, the rate of vaporization per unit volume and time, denoted by G is given by

$$G = \frac{6S}{D_p} \frac{\rho_p}{\tilde{\rho}_p} \frac{h_p}{\lambda} (T - T_s) \qquad (1)$$

where it is assumed that the particles, represented by an average spherical diameter D_p and a shape factor S, vaporize at a rate proportional to the local mean driving temperature $(T - T_s)$ and the heat transfer coefficient h_p is based on the surface area of a particle, $\pi D_p^2 S$. The energy sink is simply $G[\lambda + C_p(T - T_s)]$.

By making the usual boundary-layer approximations and integrating the resulting equations across the boundary layer, or by making mass, momentum, and energy balances across an element of volume extending into the free stream the following integral equations may be written for the conservation of momentum and energy at a point x along the flat plate.

mixture momentum:

$$\mu \left.\frac{\partial u}{\partial y}\right|_{y=0} = \frac{d}{dx}\int_0^{\delta_m} \rho_t U^2 \frac{u}{U}\left(1 - \frac{u}{U}\right) dy \qquad (2)$$

vapor energy:

$$q_w = \frac{d}{dx}\int_0^{\delta_t} \rho_v C_p u(T - T_s)dy + \int_0^{\delta_t} G \lambda \, dy \qquad (3)$$

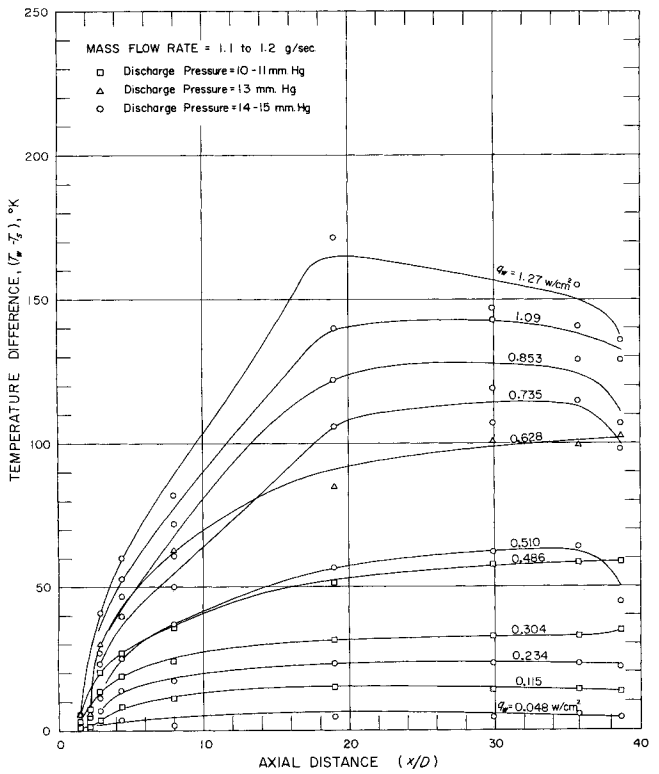

Fig. 5. Experimental temperature difference profiles for hydrogen with q_w as parameter—high flow rate.

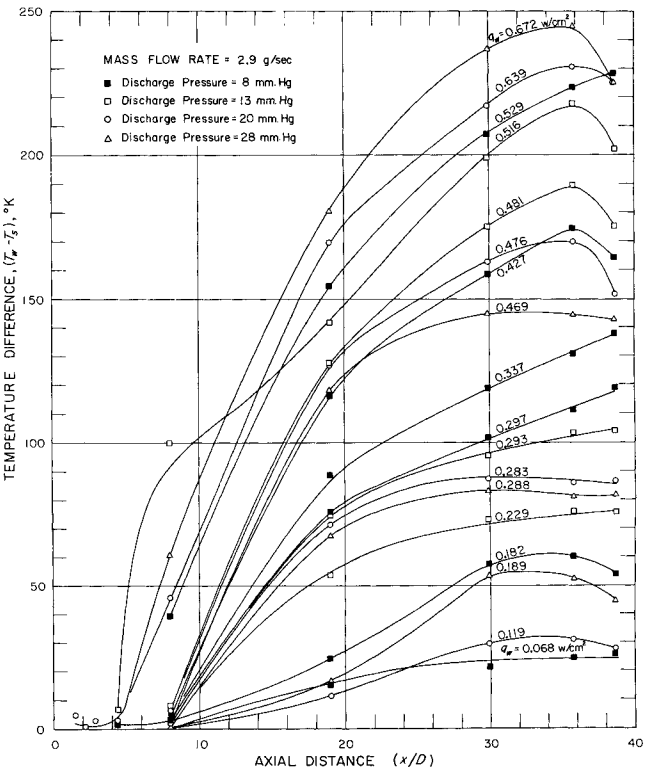

Fig. 6. Experimental temperature difference profiles for nitrogen with q_w as parameter—low flow rate.

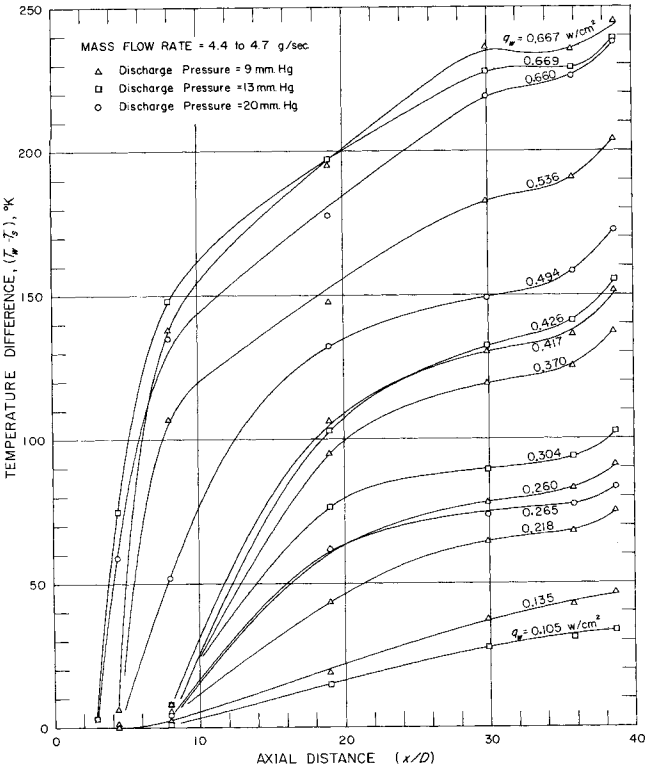

Fig. 7. Experimental temperature difference profiles for nitrogen with q_w as parameter—high flow rate.

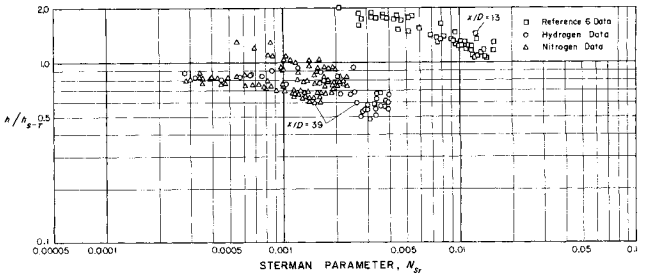

Fig. 8. Enhancement factor based on Sieder-Tate equation for hydrogen with x/D as parameter.

These are the basic equations which were applied to the two extreme cases of particle geometrical distribution.

Case 1. Uniform Particle Phase Density (ρ_p = const.)

Fourth-order polynomials were used for both temperature and velocity profiles. By satisfying the required boundary conditions the constants may be determined and when substituted into Equation (2) and (3) give, after integration, the momentum and thermal boundary-layer thicknesses of Equations (4) and (5)

$$\delta_m = \left[34 \; x \left(\frac{\mu}{\rho_t U} \right) \right]^{1/2} \tag{4}$$

$$q_w = \frac{d}{dx} \left[\rho_v C_p U \Gamma \delta_t \left\{ \Delta \left(\frac{2}{15} + \frac{17}{90} c \right) - \Delta^3 \left(\frac{3}{140} - \frac{3}{1260} c \right) + \Delta^4 \left(\frac{1}{180} - \frac{98}{27{,}216} c \right) \right\} \right] + G_w \lambda \delta_t \left(\frac{3}{10} - \frac{c}{60} \right) \tag{5}$$

where $\Delta = \delta_t/\delta_m$ and c is the coefficient of the second-order term of the temperature profile. Γ is defined as $T_w - T_s$. It can be readily shown that

$$c = \frac{\delta_t^2}{\Sigma^2}$$

where

$$\Sigma^2 = \frac{D_p^2}{3 N_{Nu,\,p} S} \frac{\lambda}{\lambda^*} \frac{\tilde{\rho_p}}{\rho_p}$$

and

$$\lambda^* = (\lambda + \Gamma C_p)$$

$c = 0$ corresponds to the usual single phase solution. If c is made a small perturbation neglect of all but terms of first order of smallness results in an explicit expression for thermal boundary-layer thickness. The result is most conveniently expressed as an enhancement factor, f, defined as the ratio of the heat transfer coefficient to that of the unperturbed single phase, the gas phase, traveling at the same free stream velocity.

$$f = (1 + \rho_p/\rho_v)^{1/6} \left[1/(1-\epsilon)^{1/3} + \frac{1}{6} (\delta_t^1/\Sigma)^2 \right] \tag{6}$$

where

$$\epsilon = (\delta_t^1/\Sigma)^2 \left[\frac{1}{5} \frac{\lambda}{\lambda^*} - 0.186 \; N_{Pr}^{1/3} (1 + \rho_p/\rho_v)^{-1/3} \right]$$

and

$$\delta_t^1 = 4.44 \; x^{1/2} \left(1 + \frac{\rho_p}{\rho_v} \right)^{-1/6} N_{Pr}^{-1/3} \left(\frac{\mu}{\rho_v U} \right)^{1/2}$$

A second simple asymptotic solution may be made for this model by taking $c >> 1$. In this case previously considered by Simpson (8), we may neglect usual convective effect of raising the gas temperature. Instead all heat is assumed to go toward vaporizing solid particles. Equation (3) becomes

$$q_w = \int_0^{\delta_t} G \lambda \, dy$$

which results quite straightforwardly from (5) in

$$f = \left(\frac{5}{6} \right)^{1/2} \left[\frac{\rho_p}{\hat{\rho_p}} N_{Nu,\,p} S \right]^{1/2} \frac{\lambda^*}{\lambda} \frac{\delta_t^0}{D_p} \tag{7}$$

where

$$\delta_t^0 = 4.44 \; x^{1/2} \; N_{Pr}^{-1/3} \left(\frac{\mu}{\rho_v U} \right)^{1/2}$$

Case 2. Vapor Film (ρ_p = 0, $y < \delta_t$; ρ_p = const., $y \geq \delta_t$)

In order to make this case tractable it was assumed from the outset that the velocity profile is the same as in case 1 and the momentum boundary-layer thickness is still given by Equation (4).

Since now, however, all vaporization is concentrated at the edge of the thermal boundary layer, the second integral in Equation (3) is zero and in its place appears q_v, the heat flux at the edge of the thermal boundary layer. Thus

$$q_w - q_v = \frac{d}{dx} \int_0^{\delta_v} \rho_v C_p \, u \, (T - T_s) \, dy \tag{8}$$

where δ_v is the new thermal boundary-layer thickness or vapor film thickness.

The following temperature profile is now introduced:

$$\frac{\theta}{\Gamma_1} = 1 - 2\eta + 2\eta^3 - \eta^4 + \Gamma_2/\Gamma_1 \, (1 - \eta), \quad \eta = y/\delta_v \tag{9}$$

where $\theta = T - T_s$

$$\Gamma_1 = (q_w - q_v)\,\delta_v/2k$$

$$\Gamma_2 = q_v\delta_v/k$$

This profile reduces to the usual single phase case when $q_v = 0$. It also satisfies all important boundary conditions although q_v remains as yet an undetermined function of x:

$$\text{At } \eta = 0, \quad \theta = \Gamma_1 + \Gamma_2, \quad \frac{-k}{\delta_v}\frac{\partial\theta}{\partial\eta} = q_w, \quad \frac{\partial^2\theta}{\partial\eta^2} = 0 \tag{10}$$

$$\text{At } \eta = 1, \quad \theta = 0 \qquad \frac{-k}{\delta_v}\frac{\partial\theta}{\partial\eta} = q_v, \quad \frac{\partial^2\theta}{\partial\eta^2} = 0$$

Velocity and temperature profiles may again be substituted into Equation (8). After integration this yields

$$q_w - q_v = \frac{\rho_v C_p U}{k}\frac{d}{dx}\left[\frac{\delta_v^2(q_w - q_v)}{2}\left(\frac{2\Delta}{15} - \frac{3\Delta^3}{140} + \frac{\Delta^4}{180}\right) + q_v\delta_v^2\cdot\left(\frac{\Delta}{3} - \frac{\Delta^3}{10} + \frac{\Delta^4}{30}\right)\right] \tag{11}$$

Neglecting all but the terms in Δ an approximate solution may again be obtained for δ_t in the case of $q_v/q_w << 1$, that is, a perturbation on the single phase case of $q_v = 0$. Under these conditions integration of (11) results in

$$f = [1 + q_v/q_w]^{-1}\,[(1 - 2q_v/q_w)/(1 + 4q_v/q_w)\,]^{-1/3} \tag{12}$$

In this approximation,

$$q_v/q_w = N_{Sr}^{-1}\,\pi(\delta_t^0/2x)\;(\rho_p/\rho_v)$$

where $\pi = (2\Delta^0 - 2\Delta^{03} + \Delta^{04})$ and Δ^0 is the single phase ratio of thermal to momentum boundary-layer thickness

$$\Delta^0 = 0.761\;N_{Pr}^{-1/3}$$

We have also introduced a dimensionless heat flux N_{Sr}, the Sterman parameter, defined as

$$N_{Sr} = \frac{q_w}{\rho_v U\lambda}$$

The resulting enhancement factors, Equations (6), (7), and (12), for the cases considered have been derived for a distance x from the commencement of the boundary layer for flow over a flat plate. The equations will also apply for some distance in the entrance region of a straight tube. For this case the more familiar Reynolds number form may be used for δ_t^0 by introducing the tube diameter, D, thus,

$$\delta_t^0/x = 4.44\;N_{Pr}^{-1/3}\,(x/D)^{-1/2}\,(N_{Re,\,v})^{-1/2} \tag{13}$$

DISCUSSION

In this discussion an attempt will be made to interpret

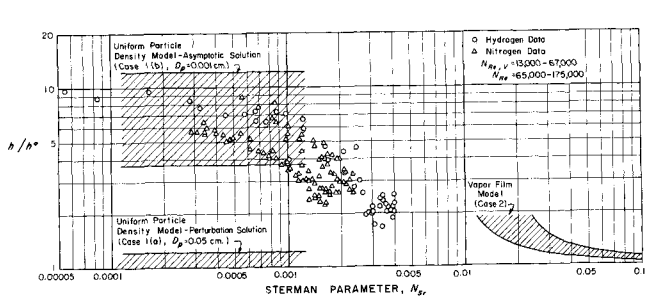

Fig. 9. Comparison of theoretical and experimental enhancement factors for $x/D = 39$—hydrogen and nitrogen.

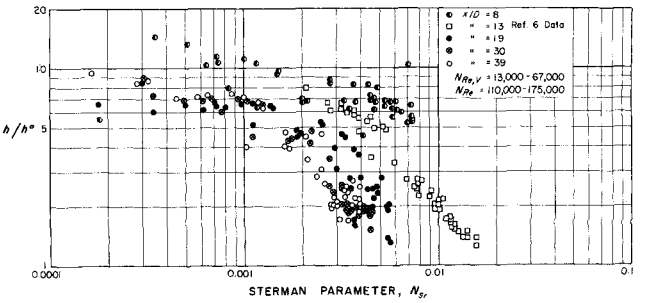

Fig. 10. Comparison of experimental enhancement factors for variation of x/D—hydrogen.

the broad features of the experimental results with reference to the theory presented. In the region close to the discharge orifice the fluid mechanical situation of the stream impinging on the tube wall with a nonequilibrium condition existing between the phases does not lend itself to analysis. The rather complex behavior noted above in Figures 4, 5, 6, and 7 in which the two fluids appear to behave differently is evidence of this. However, it is supposed that adjacent to the wall a laminar boundary layer does begin to develop in some manner in the region of the orifice. It is further expected that the development of the boundary layer becomes less dependent on this orifice condition the farther one proceeds down the tube, so that the wall temperatures or heat transfer coefficients here should be amenable to analysis.

The temperature difference profiles of Figures 4, 5, 6, and 7 show typical single-phase behavior away from the orifice except for erratic behavior near the end of the tube. (This amounts to a small percentage since here the temperature differences are high.) Theory predicts, however, that the heat transfer coefficient should be enhanced by the presence of vaporizing solid. Unfortunately, it was not possible in these experiments to measure heat transfer coefficients for the single phase, pure gas case under comparable conditions and therefore calculation is the only recourse.

It was suggested in a previous paper (6) by a dimensional analysis that, for a given value of x/D, a correlation should exist between the enhancement factor, $f = h/h^0$, and the Sterman parameter N_{Sr}. While the present theory qualifies this somewhat, the plot is still convenient in that one can say something about the trend to be expected, namely: at large values of N_{Sr}, f should decrease to an asymptotic value of 1.0 for all values of x/D. This is the prediction according to Equation (12) and, in words, means simply that for high heat flux the tube wall becomes blanketed by a thick layer of gas which, in the limit, becomes pure gas flow as all the solid is vaporized.

If fully developed turbulent flow existed toward the end of the tube the Sieder-Tate correlation

$$h_{S\text{-}T} = 0.026\,(k/D)\,N_{Re}^{0.8}N_{Pr}^{0.33}\,(\mu_s/\mu_w)^{0.14} \tag{14}$$

could be used to calculate the heat transfer coefficient, h^0, for the pure gas traveling at the same velocity as the mixture. The enhancement factor so calculated is shown in Figure 8 plotted against N_{Sr} for $x/D = 39$. Also shown are the data from a previous paper (6) for $x/D = 13$. Apparently the Sieder-Tate correlation overpredicts the equivalent pure gas heat transfer coefficient since the enhancement factor for $x/D = 39$ approaches a value of 0.5 to 0.6. The data for $x/D = 13$ approach 1.0 as was noted elsewhere (6), but it now seems likely that part of the enhancement here when compared to fully developed turbulent flow is due to this station's being higher in the entrance region.

In the theory presented in this paper it is suggested that laminar boundary-layer theory could be used to describe the developing wall temperatures. In Figure 9 the enhancement factor presented was calculated for $x/D = 39$ using for h^0 the value obtained from Equation (14) for pure vapor traveling at the same free stream velocity as the mixture. Transport properties were calculated at $T = (T_w + T_s)/2$. The enhancement factor calculated in this way is now compatible with the stated requirement at large values of N_{Sr} for $x/D = 39$. For all other values of x/D, f is greater than 1.0 also and shows the correct trend of decreasing as N_{Sr} increases. It is noted also in this figure that the data for hydrogen and nitrogen correlate well.

According to Schlichting (7) the transition of a laminar to a turbulent boundary layer takes place over a flat plate at a Reynolds number based on length of the order of 3×10^5. In the present experiments this value is often exceeded toward the end of the tube and, indeed, some of the erratic behavior of the temperature difference profiles, particularly at high heat fluxes, could be explained by this; the possibility should not be excluded that at low heat flux the unvaporized particles in the boundary layer damp out turbulent fluctuations and therefore stabilize the flow. In either case it is clear from Figures 8 and 9 that fully developed turbulence was not attained in these experiments, and the laminar boundary-layer calculation of h^0 is at least a reasonable upper limit.

It now appears that, except at high values of N_{Sr}, heat transfer is enhanced by the presence of subliming particles; indeed, according to Figure 9, up to a tenfold enhancement was realized.

Theoretical values of f are also shown on Figure 9. At high values of N_{Sr}, f was calculated for $x/D = 39$ and the range of N_{Re} encountered experimentally using Equation (12) for the vapor film model. Unfortunately, the range of validity of the calculation does not encompass the experimental data, but it appears that this model could represent the correct asymptotic behavior for large values of N_{Sr}. In any case the trend of f with N_{Sr} is given a qualitative description. The uniform particle density model was applied using the extreme values of particle sizes observed. For the 500μ particles the perturbation calculation of Equation (6) is valid, and the result is the lower shaded area at the left of the figure. For 10μ particles the perturbation term, c, is too large for Equation (6) to be valid. However, this case may be handled by the asymptotic solution, Equation (7). This is represented by the upper shaded area at the left of the figure. These two results have been plotted at low N_{Sr} because this is precisely where uniform density is expected, that is, low heat flux and, consequently, no vapor film.

The result obtained for the enhancement factor from the asymptotic solution is in good agreement with experiment at low values of N_{Sr}. Since it is also at low N_{Sr} that temperature profiles are flat as required by the model it is felt that the asymptotic solution adequately describes the low heat flux process. The perturbation solution is either inapplicable (small particles) or predicts too low an enhancement (large particles). It is evident that particle size data are crucial if the enhancement factor is to be accurately predicted, but it is felt that these results using a wide range of particle size are at least encouraging.

The preceding discussion leads to the following interpretation of the observed trend of f with N_{Sr}. At low heat flux and hence low N_{Sr} the distribution of particles is unperturbed by vaporization and is therefore independent of N_{Sr} as predicted by the uniform density model. Increasing N_{Sr} vaporizes particles from the region adjacent to the wall forming some sort of film as particle concentration is depleted. Although the discontinuous concentration profile used in the vapor film model is not realistic, it is felt nevertheless that the same interpretation can be given to the role of N_{Sr} as is indicated theoretically, namely, N_{Sr} is an index of the departure of particle concentration profile from uniform. A striking confirmation of this interpretation is obtained from the photographs, Figures 2 and 3 of the solid vapor stream emerging from the end of the heated tube. In Figure 3, N_{Sr} is 2.3 times the value in Figure 2; all other conditions are comparable.

A further point of interest is the dependence of the enhancement factor on position along the tube. This is illustrated in Figure 10 for hydrogen data at $x/D = 8$, 19, 30, and 39. Also presented for comparison are the data for $x/D = 13$ from (6). The two sources of data seem to be reasonably compatible.

ACKNOWLEDGMENT

This work was supported by the National Aeronautics and Space Administration (Space Nuclear Propulsion Office) under Contract R-45. A. U. Simpson was Research Associate with the Cryogenics Division, National Bureau of Standards-Institute for Materials Research from February, 1966 to August, 1967 under the sponsorship of AiResearch Manufacturing Division of the Garrett Corporation.

NOTATION

c = coefficient of η^2 in dimensionless temperature profile
C_p = constant pressure specific heat vapor, J/g°K.
D = inside tube diameter, cm.
D_p = average spherical particle diameter, cm.
f = enhancement factor
F = force on particle, dynes
G = rate of vaporization per unit volume, g./cc.sec.
h = local heat transfer coefficient, W/sq.cm.°K.
h_p = particle heat transfer coefficient, W/sq.cm.°K.
k = vapor thermal conductivity, W/cm.°K.
N_{Nu} = Nusselt number, hD/k
$N_{Nu,\,p}$ = particle Nusselt number, h_pD_p/k
N_{Pr} = Prandtl number, $\mu C_p/k$
N_{Re} = Reynolds number, $(\rho_p + \rho_v)UD/\mu$
$N_{Re,\,v}$ = Reynolds number, ρ_vUD/μ
N_{Sr} = Sterman parameter $q_w/\rho_vU\lambda$
q_v = heat flux at vapor film boundary, W/sq.cm.
q_w = heat flux through tube wall, W/sq.cm.
S = shape factor (surface area of particle/πD_p^2)
T = local mean temperature of vapor, °K.
T_w = local inside wall temperature, °K.
T_s = local saturation temperature, °K.
u = axial velocity component, cm./sec.
U = free stream velocity for flat plate analysis, cm./sec.
v = radial velocity component, cm./sec.
x = axial distance along flat plate, cm.
y = perpendicular distance from wall, cm.

Greek Letters

Γ = temperature difference $T_w - T_s$, °K.
Γ_1 = $(q_w - q_v)\,\delta_v/2k$, °K.
Γ_2 = $q_v\delta_v/k$, °K.
δ_m = momentum boundary layer thickness, cm.
δ_t = thermal boundary layer thickness, cm.
δ_v = vapor film thickness, cm.
Δ = δ_t/δ_m or δ_v/δ_m
ϵ = perturbation constant
η = dimensionless coordinate (y/δ_t)
θ = temperature difference $T - T_s$, °K.
λ = latent heat of sublimation, J/g.
μ = vapor viscosity, g./sec.cm.
ξ = dimensionless coordinate (y/δ_m)

π = dimensionless function of Prandtl number

$\tilde{\rho}_p$ = average solid particle phase density, g./cc.

ρ = specific density of solid, g./cc.

ρ_t = total density $(\rho_p + \rho_v)$, g./cc.

ρ_v = density of vapor, g./cc.

Σ = $[(D_p^2/3N_{Nu,p} \cdot S)(\lambda/\lambda^*)(\tilde{\rho}_p/\rho_p)]^{1/2}$, cm.

Subscripts

m = momentum

p = particle

s = saturation conditions

t = thermal

v = vapor or vapor film

w = wall conditions

Superscripts

0 = unperturbed pure vapor phase

1 = two-phase without vaporization

LITERATURE CITED

1. Farbar, L., and C. A. Depew, *Ind. Eng. Chem. Fundamentals*, **2**, 130 (1963).
2. Tien, C. L., and V. Quan, *Am. Soc. Mech. Eng., paper No. 62-HT-65*, 1 (1962).
3. Abel, W. T., D. E. Bluman, and J. P. O'Leary, *ASME paper No. 63-WA-210* (1963).
4. Tien, C. L., *J. Heat Transfer*, **83**, 183 (1961).
5. Edelman, R. B., Ph.D. thesis, Yale Univ., New Haven, Conn. (1962).
6. Jones, M. C., T. T. Nagamoto, and J. A. Brennan, *AIChE J.*, **12**, 790 (1966).
7. Schlichting, H., "Boundary Layer Theory," 4th Ed., McGraw-Hill, New York (1960).
8. Simpson, A. U., Ph.D. thesis, Univ. Colorado, Boulder (1967).

Manuscript received May 10, 1968; revision received August 1, 1968; paper accepted August 5, 1968.

Simultaneous Flow and Temperature Correction in the Equilibrium Stage Problem

JOHN W. TIERNEY and JOHN L. YANOSIK

University of Pittsburgh, Pittsburgh, Pennsylvania

Iterative methods for the solution of the steady state equilibrium stage problem are studied. Equations are first developed for calculating the effect of a change in temperature or flow rate on all energy balances, and then it is shown that these equations can be used in the multiple variable form of the Newton-Raphson correction process to correct either the temperatures or the flow rates when only energy balance errors are used. Similar equations for material balance errors which have been developed previously are then combined with the energy balance equations to provide a method for simultaneous correction of the temperatures and the flow rates. Because first-order interactions between flow rates and temperatures are included the method is applicable to a wide range of equilibrium stage problems. Sample problems are presented, and it is shown that quadratic convergence is obtained for the simultaneous correction process.

The solution of the equilibrium stage problem is of both historical and practical importance to chemical engineers. Over the years many methods have been proposed, such as analytic solutions, graphical solutions, and numerical approximations. In the last few years there has been an emphasis on numerical methods because of the availability of large computing machines. In a previous paper (*1*) it was pointed out that the computer solution is usually stated as that of finding a set of temperatures and flow rates which will satisfy all material and energy balances. For a system with n stages, there are n temperatures and n flow rates to be fixed, and there are n material balances and n energy balances to be satisfied. Direct solution is not possible, and iterative methods are used. At each step of the iterative process the material balance and energy balance errors are reduced by correcting the temperatures and flow rates. A linear correction process can be defined as:

$$(\Psi) \begin{bmatrix} C_t \\ C_v \end{bmatrix} = - \begin{bmatrix} D_m \\ D_e \end{bmatrix} \qquad (1)$$

where (C_t, C_v) is a vector containing the corrections to be made in the temperatures and flow rates, and (D_m, D_e) is a vector containing the material balance errors and energy balance errors. Ψ is the correction matrix. There are many ways in which Ψ can be defined, but in this paper it will be the Jacobian matrix of the errors. It can be shown that the Jacobian matrix will give quadratic convergence in the vicinity of the solution, and this is the most rapid convergence possible with a linear correction